

Electrochemical Behavior and Electrolytic Separation of Nd in the LiF-NaF-KF Molten Salt System

Authors: Lei Min, Zheng Bowen, Xu Tongtong, Qiu Jie

Date: 2025-04-21T10:07:04+00:00

Abstract

The electrolytic separation of neodymium, a fission product in thorium-based molten salt reactors, is of great significance for the long-term stable operation of molten salt reactors, improvement of fuel utilization efficiency, and reduction of radioactive waste. Focusing on the electrolytic separation characteristics of neodymium in molten salt environments, this study investigates the electrochemical behavior and thermodynamic properties of NdF₃ in the FLiNaK(46.5:11.5:42 mol%) molten salt system within the temperature range of 873~933K. The results demonstrate that the reduction of Nd(III) to neodymium metal on an inert tungsten electrode is a one-step process, namely $\text{Nd(III)} + 3\text{e}^- \rightarrow \text{Nd(0)}$. Furthermore, the diffusion coefficient D of Nd(III) ions in the molten salt was determined through cyclic voltammetry, revealing that D increases with temperature. The activation energy of Nd(III) in the molten salt is $174.49 \text{ kJ} \cdot \text{mol}^{-1}$. The open-circuit chronopotentiometric curves were utilized to obtain the equilibrium electrode potential and apparent electrode potential of the Nd(III)/Nd(0) system within the temperature range of 873K~933K. Finally, at 873K, pulse electrolytic deposition experiments of Nd were conducted, with the electrodeposits analyzed by X-ray diffraction (XRD) and the molten salt before and after electrolysis analyzed by inductively coupled plasma optical emission spectrometry (ICP-OES). The successful detection of metallic Nd deposition and a significant reduction in neodymium ion content demonstrates that pulse electrolysis is a viable method for separating neodymium from molten fluoride salt systems.

Full Text

Electrochemical Behavior and Electrolytic Separation of Nd in LiF-NaF-KF Molten Salt

Lei Min¹, Zheng Bowen², Xu Tongtong³, Qiu Jie^{1*}

¹ School of Nuclear Science and Technology, Xi'an Jiaotong University, Xi'an 710049, China

² China Institute of Radiation Protection, Taiyuan 030000, China

³ School of Energy and Power Engineering, Xi'an Jiaotong University, Xi'an 710049, China

Corresponding author. Email: qiu2021@xjtu.edu.cn

Abstract

The electrolytic separation of neodymium (Nd), a fission product in thorium-based molten salt reactors (TMSR), is crucial for ensuring long-term reactor stability, enhancing fuel utilization, and minimizing radioactive waste. This work investigates the electrochemical behavior and thermodynamic properties of NdF₃ in the FLiNaK (46.5:11.5:42 mol%) molten salt system across the temperature range of 873–933 K. Results demonstrate that Nd(III) undergoes a single-step reduction to metallic Nd on inert tungsten electrodes via the reaction $\text{Nd(III)} + 3\text{e}^- \rightarrow \text{Nd(0)}$. Cyclic voltammetry measurements reveal that the diffusion coefficient (D) of Nd³⁺ increases with temperature, yielding an activation energy of 174.49 kJ·mol⁻¹. Open-circuit chronopotentiometry was employed to determine the equilibrium electrode potential and apparent electrode potential for the Nd(III)/Nd(0) couple between 873 K and 933 K. Finally, pulsed electrolytic deposition experiments conducted at 873 K, combined with X-ray diffraction (XRD) analysis of the deposits and inductively coupled plasma optical emission spectroscopy (ICP-OES) analysis of the melt before and after electrolysis, successfully confirmed metallic Nd deposition and a significant reduction in neodymium ion concentration, proving that pulsed electrolysis is a viable method for separating Nd from molten fluoride salt systems.

Keywords: Electrochemistry; FLiNaK salt; Nd(III)/Nd(0); Diffusion coefficient; Electrodeposition

Funding: This work was supported by the Research Project of Shaanxi Province (Grant No. 2023SYJ18).

1. Introduction

Advanced thorium-based molten salt reactors (TMSR) utilize Th-232 as the primary fertile fuel, which can be converted to fissile U-233 through neutron capture and subsequent β -decay [1]. In addition to thorium, spent fuel from TMSR operations contains significant concentrations of fission products and trace amounts of uranium. Among these, cerium (Ce), neodymium (Nd), and samarium (Sm) are the three most abundant fission product elements. Accumulation of these fission products in the molten salt reduces reactor efficiency, alters salt fluidity, increases viscosity, and ultimately compromises the safety and sustainability of the reactor system [2, 3]. Furthermore, neodymium serves as a critical component in rare-earth permanent magnet materials such as NdFeB, for which global demand is substantial and resources are scarce [4, 5]. Therefore, the electrolytic separation of neodymium from spent nuclear fuel represents a key step toward realizing a nuclear energy circular economy, offering simultaneous benefits in resource recovery, environmental protection, and technological innovation.

Fluoride molten salts are employed as both fuel and coolant salts in TMSR due to their exceptional thermochemical properties, including low thermal neutron absorption cross-section, high heat capacity, excellent fluidity and thermal conductivity, wide liquid operating range, and good chemical stability [6, 7]. The nuclear fuel, in the form of fluorides (ThF_4 , UF_4 , or TRUF), is uniformly dissolved in a carrier salt composed of LiF (with ^7Li enrichment $>99.95\%$) and BeF_2 , creating a flowable liquid nuclear fuel without fixed geometry that enables online or offline fuel processing and cycling during reactor operation [3, 7]. The electrolytic separation of fission products (Ce, Nd, and Sm) from molten salt reactor fuel constitutes a core component of closed fuel cycle implementation.

In recent years, numerous experimental studies have investigated the electrochemical behavior of Nd(III) in chloride molten salts, including LiCl-KCl [8–10], NaCl-CaCl₂ [11], and LiCl-CaCl₂ systems [10, 12]. Yamana et al. [8] first demonstrated stable generation of divalent neodymium (Nd^{2+}) in LiCl-KCl melts, showing that Nd^{2+} formation is closely related to Cl^- concentration and potential control. Tang et al. [9] systematically studied the reduction kinetics of Nd^{3+} on molybdenum electrodes, finding that Nd deposition follows an instantaneous nucleation mode with deposition rates significantly influenced by temperature and concentration. Vandarkuzhali et al. [10] examined the effects of different electrode materials (W, Al, Cd) on the electrochemical behavior of NdCl_3 in LiCl-KCl melts, observing a two-step reduction ($\text{Nd}^{3+} \rightarrow \text{Nd}^{2+} \rightarrow \text{Nd}^0$) on aluminum electrodes but only a single-step reduction ($\text{Nd}^{3+} \rightarrow \text{Nd}^0$) on tungsten and cadmium electrodes. Novoselova et al. [13] investigated the electrochemical behavior of NdCl_3 in LiCl-KCl-CsCl eutectic using cyclic and linear sweep voltammetry, determining the apparent standard redox potentials for Nd(III)/Nd(II) and Nd(0).

In contrast to chloride melts, experimental results on the electrochemical be-

havior of Nd(III) in fluoride molten salts are relatively scarce. Stefanidaki et al. [14] studied the electrochemical behavior and electrode reaction processes in LiF-NdF₃, LiF-Nd₂O₃, and LiF-NdF₃-Nd₂O₃ systems using cyclic voltammetry, finding that neodymium fluoride is reduced from LiF-NdF₃-Nd₂O₃ melts as NdO on the electrode substrate while neodymium oxyfluoride is oxidized to oxygen at the anode. Moriyama et al. [15] measured equilibrium distributions of Nd(III) with liquid metals Bi, Sn, Cd, and Zn in LiF-BeF₂ binary phase systems at temperatures from 600°C to 800°C. Rault et al. [16] obtained optimal separation coefficients for actinides and Nd in molten fluoride salts using LiF-AlF₃ two-phase melts. Gibilaro et al. [17] studied the reduction process of Al-Nd in LiF-CaF₂ medium (79–21 mol%) at 860°C, demonstrating that Nd can co-deposit with Al as intermetallic compounds (Al₁₁Nd₃, Al₃Nd, AlNd₂, and AlNd₃) on electrodes with electrolytic efficiency exceeding 95%. Chamelot et al. [18] found that all high-lanthanide-content Ln-Ni intermetallic compounds could be obtained in liquid form at moderate temperatures during electrochemical separation/extraction of lanthanides on nickel electrodes, enabling determination of separation efficiency for each lanthanide element in the melt.

Although a one-step reduction mechanism from Nd(III) to Nd(0) has been confirmed in various fluoride melts such as LiF, LiF-KF, and LiF-CaF₂—markedly different from the reduction mechanism in chloride melts—Soucek et al. [19] observed no redox peaks for Nd(III) on platinum working electrodes in the LiF-NaF-KF (FLiNaK) system. This suggests that both electrode material and melt composition may significantly influence the electrochemical behavior of Nd. Therefore, further investigation of Nd electrochemistry in high-temperature fluoride melts is necessary to elucidate the electrode reaction mechanism and optimize the electrolytic separation process. This study systematically examines the redox behavior of Nd(III) on tungsten electrodes in the LiF-NaF-KF (46.5:11.5:42 mol%, FLiNaK) molten salt system between 873 K and 933 K. Through cyclic voltammetry and square wave voltammetry, we observe a one-step reduction process $\text{Nd(III)} + 3\text{e}^- \rightarrow \text{Nd(0)}$ on W electrodes. We systematically measure diffusion coefficients and apparent standard potentials of Nd(III) at various temperatures, calculating an activation energy of 174.49 kJ · mol⁻¹. Following four-stage pulsed electrolysis, metallic Nd is successfully deposited on the tungsten electrode surface.

2. Experimental

2.1 Materials and Preparation

All chemicals used in this study were purchased from Aladdin: LiF (99.9% metal basis), NaF (99.99% metal basis), KF (99.9% metal basis), and NdF₃ (99.99% metal basis). A 50 g FLiNaK sample was prepared according to the molar ratio LiF-NaF-KF (46.5:11.5:42 mol%) and doped with 3 wt.% NdF₃. The mixture was homogenized using a stirrer and placed in a 100 mL nickel

crucible. To remove residual moisture and oxygen, the mixture was held at 673 K for 24 hours, then heated to the experimental temperature and maintained for 4 hours prior to electrochemical testing. All operations were performed in an argon-atmosphere glove box with water and oxygen contents below 1 ppm.

2.2 Electrochemical Characterization of Nd(III)

Electrochemical measurements were conducted using a Gamry Interface 1010E potentiostat with a conventional three-electrode system. A graphite rod (ϕ 5 mm \times 150 mm, Alfa-Aesar) served as the counter electrode (CE), a tungsten rod (ϕ 5 mm \times 150 mm, Merson) as the working electrode (WE), and a platinum rod (ϕ 2 mm \times 150 mm, Alfa-Aesar) as the reference electrode (RE). After melting the FLiNaK salt, electrodes were immersed to a depth of 7 mm for subsequent measurements. The electrochemical behavior of Nd(III) in NdF₃-FLiNaK melts was investigated using cyclic voltammetry (CV, potential range: 0–2.0 V, scan rates: 0.1–0.8 V/s), chronopotentiometry (CP, current range: –40 to –50 mA), and square wave voltammetry (SWV, scan rate: 0.1 V/s, frequency: 25 Hz).

2.3 Electrolytic Deposition of Nd from NdF₃-FLiNaK Melts

Pulsed potential electrolysis was employed for Nd deposition from NdF₃-FLiNaK melts. Each pulsed electrolysis cycle comprised four stages: (1) application of a potential more negative than the Nd(III) deposition potential for a short duration to locally concentrate electroactive species at the electrode surface; (2) application of a deposition potential slightly more negative than the Nd(III) reduction potential for Nd deposition; (3) application of a slightly positive voltage for a brief period to convert the cathode to an anode, partially redissolving the loose deposit layer; and (4) application of a stable voltage to minimize electrode surface disturbance and reduce further deposition/dissolution of Nd between the electrode and bulk melt.

2.4 Analysis of Electrolysis Products and Ion Concentrations

Following high-temperature pulsed electrolysis, substantial electrolysis products accumulated on the working electrode surface. The electrode was extracted at high temperature and cooled naturally, with cathode products collected inside the argon-filled glove box. Electrolysis products were analyzed using a Bruker D8 Advance X-ray diffractometer equipped with Cu K α radiation ($\lambda = 1.54184$ Å) at 40 kV and 40 mA. Diffraction parameters were set as follows: 2 θ range 10°–90°, scan speed 8°/min. To analyze Nd(III) ion content, samples were taken from different positions of the cooled melt (edge 1, edge 2, and center) after electrolysis and compared with pre-electrolysis concentrations. Due to non-uniform ion distribution in the solidified salt, 0.1 g samples were dissolved in 10 mL nitric acid and diluted to 100 mL for analysis using a PRODIGY 7 inductively coupled plasma optical emission spectrometer (ICP-OES).

3. Results and Discussion

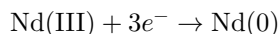
3.1 Redox Behavior of Nd in NdF₃-FLiNaK Melts

The redox processes of NdF₃ (3 wt.%) in FLiNaK melts between 873 K and 933 K were investigated using cyclic voltammetry, with results shown in Figure 1 [Figure 1: see original paper]. The gray curve for the blank FLiNaK melt exhibits only one redox couple at approximately -1.87 V/-1.93 V, corresponding to the Li(I)/Li(0) redox pair. Upon addition of NdF₃ to the FLiNaK melt, a new redox peak pair b/b' appears near -1.41 V/-1.67 V, associated with Nd metal deposition and dissolution. This indicates that Nd(III) reduction to Nd(0) occurs in a single step. The oxidation peak at -0.892 V (peak c) likely originates from impurities, while the pronounced rise at the end of the cyclic voltammogram (feature d) corresponds to fluorine gas evolution [20]. Cyclic voltammograms collected across 873-933 K (Figure 1a) show that increasing temperature has minimal effect on the redox potentials.

Square wave voltammetry (SWV) offers more sensitive detection of redox reactions and facilitates kinetic studies through its reversibility and rapid scanning capability, enabling calculation of electron transfer numbers. Figure 1b presents SWV curves for NdF₃ (3 wt.%) - FLiNaK melts scanned at 25 Hz in the low-potential region. Based on Figure 1a, peak a' (-1.93 V) corresponds to Li(I) reduction to Li(0), while signal b' (-1.67 V) represents Nd(III) reduction to Nd(0). Scanning the voltage range of the Nd(III) reduction peak b' and applying Gaussian fitting yields a half-peak width of 0.08986 V. Combining this with Equation (1) allows estimation of the electron transfer number [21]:

$$W_{1/2} = \frac{3.52RT}{nF}$$

where $W_{1/2}$ is the half-peak width, n is the electron transfer number, T is temperature (K), F is the Faraday constant ($C \cdot \text{mol}^{-1}$), and R is the gas constant ($J \cdot \text{mol}^{-1} \cdot \text{K}^{-1}$). The estimated n value of approximately 2.95, close to 3, confirms that the Nd(III)/Nd(0) reduction proceeds via a one-step, three-electron transfer process, consistent with previous reports [10, 15, 16]. Therefore, the electrode reaction for Nd(III) ions in FLiNaK melts can be described as:



3.2 Diffusion Behavior of Nd(III) in NdF₃(3 wt.%) - FLiNaK Melts

The diffusion coefficient serves as a critical parameter for assessing ion mobility during electrode reactions, as diffusion often constitutes the rate-limiting step in most electrochemical processes and ultimately affects electrolytic efficiency. This work provides detailed measurements of Nd(III) diffusion coefficients in FLiNaK melts. However, significant variations in diffusion coefficients arise due

to differences in cathode passivation. Two distinct calculation methods were employed: chronopotentiometry (CP), which exhibits milder electrode passivation, and cyclic voltammetry (CV), which shows more severe passivation phenomena [22].

Figure 2a [Figure 2: see original paper] shows CP curves for the NdF_3 (3 wt.%)–FLiNaK melt system, with applied currents ranging from -50 to -100 mA. A distinct redox process appears near -1.60 V, corresponding to the Nd(III) reduction potential. The transition time (τ) of the plateau varies with the applied current, where larger currents produce longer τ values, while the onset of the reduction potential remains current-independent. This behavior indicates that the electrode reaction of Nd(III) in FLiNaK melts is diffusion-controlled. Based on the Sand equation (3), a linear relationship exists between the applied current and $\tau^{-1/2}$ (Figure 3b [Figure 3: see original paper]), enabling calculation of the Nd(III) diffusion coefficient [23]:

$$I = 0.5nFSC_{\text{Nd(III)}}\sqrt{\frac{D_{\text{Nd(III)}}}{\pi\tau}}$$

where I is the set current (A), τ is the transition time, n is the number of electrons transferred (3), F is the Faraday constant, S is the electrode area, and $C_{\text{Nd(III)}}$ is the Nd concentration. Analysis of the chronopotentiometric data yields a Nd(III) diffusion coefficient of $5.26 \times 10^{-6} \text{ cm}^2 \cdot \text{s}^{-1}$ at 873 K.

Figure 3 [Figure 3: see original paper] presents cyclic voltammograms for NdF_3 ($2.27 \times 10^{-4} \text{ mol/cm}^3$)–FLiNaK at scan rates from 0.1 to 0.8 V/s. To verify reaction reversibility, peak potential versus scan rate was plotted (Figure 3b), showing negligible peak potential shift across different scan rates, confirming reversibility. The Nd redox peaks increase with scan rate, and the relationship between peak current and the square root of scan rate is linear (Figure 3c): $I_p = 0.025 - 0.115\sqrt{v}$ with $\text{adj-}R^2 = 0.9994$, indicating diffusion-controlled reduction of Nd(III)/Nd(0). For diffusion-controlled reactions, the diffusion coefficient can be calculated using the Berzins and Delahay (B&D) equation (4) [24]:

$$i_p = 0.61(nF)^{3/2}AC_0\sqrt{\frac{D_{\text{Nd(III)}}v}{RT}}$$

where i_p is the cathodic peak current, n is the electron transfer number, F is the Faraday constant (96485 C/mol), R is the gas constant [8.314 J/(mol · K)], T is absolute temperature (K), A is the effective electrode area (1.1304 cm^2), C_0 is the initial NdF_3 concentration ($2.27 \times 10^{-4} \text{ mol/cm}^3$), $D_{\text{Nd(III)}}$ is the diffusion coefficient (cm^2/s), and v is the potential scan rate. Substituting the slope from the linear relationship between cathodic peak current and \sqrt{v} into Equation (4) yields a Nd(III) diffusion coefficient of $2.17 \times 10^{-7} \text{ cm}^2/\text{s}$ in FLiNaK melts at 873 K. This value is one order of magnitude smaller than that obtained

from CP measurements due to more severe electrode passivation during CV, consistent with observations in other molten salt systems [22].

3.3 Diffusion Activation Energy of Nd(III) in NdF₃(3 wt.%)–FLiNaK Melts

The temperature dependence of Nd(III) diffusion coefficients in FLiNaK melts was investigated. To avoid complications from varying cathode passivation, cyclic voltammetry was used exclusively for diffusion coefficient measurements between 893 K and 933 K. Table 1 summarizes the calculated diffusion coefficients $D_{\text{Nd(III)}}$ at different temperatures based on CV data from Figures 3–4 and Equation (4). The results show that both the redox potential and diffusion coefficient shift positively and increase, respectively, with temperature. This trend arises because elevated temperature increases molecular average kinetic energy (following Maxwell-Boltzmann distribution) and accelerates ionic motion [9, 10].

Diffusion processes must overcome an “energy barrier,” with activation energy being the key limiting factor. Increased temperature enhances molecular kinetic energy, lowering this energy threshold and significantly accelerating diffusion. The temperature dependence of diffusion in ideal solutions typically follows the Arrhenius equation [25], establishing the following relationship between diffusion coefficient D and temperature T :

$$D = D_0 \exp\left(-\frac{E_a}{RT}\right) \quad \text{or} \quad \ln D = \ln D_0 - \frac{E_a}{RT}$$

where E_a is the diffusion activation energy ($\text{J} \cdot \text{mol}^{-1}$), D_0 is the pre-exponential factor, and $\ln D$ ($\text{cm}^2 \cdot \text{s}^{-1}$) exhibits a linear relationship with $1/T$ (K^{-1}), allowing determination of E_a from the slope. From Figure 7 [Figure 7: see original paper], the slope $k = -20988.02$ yields a diffusion activation energy of approximately **174.49 kJ · mol⁻¹** for Nd(III) in the NdF₃(3 wt.%)–FLiNaK system. According to the Arrhenius relationship, decreasing E_a (or increasing temperature) significantly enhances the reaction rate constant D_0 . Combined with the Butler-Volmer equation, this process increases the exchange current density j_0 of the cathodic reaction. In the limiting diffusion current region, current density is diffusion-controlled, and the synergistic effect of activation energy and diffusion coefficient ultimately determines the overall electrochemical reaction rate.

3.4 Apparent Standard Potential

The apparent standard potential is essential thermodynamic data for studying ionic electrochemical reactivity in molten salts and serves as an indicator of electrochemical properties and relative oxidation/reduction strength [26]. More positive potentials indicate stronger oxidation capability of the oxidized species,

while more negative potentials indicate stronger reduction capability of the reduced species. Additionally, the difference between standard potentials can determine whether species can be separated via electrolysis [27]. Since most molten salt systems deviate from standard conditions and lack comprehensive standard potential databases, and because nucleation overpotentials preclude the use of transient electrochemical techniques for measuring apparent standard potentials, we employed electromotive force measurements to determine these values [28].

At various temperatures, tungsten electrodes were coated with metallic Nd by applying cathodic current for 30 s, and the open-circuit potential (OCP) relative to a Pt reference electrode was recorded until a stable plateau was obtained, representing the equilibrium potential E_{eq} . The relationship between standard electrode potential E^0 , equilibrium potential E_{eq} , and apparent standard electrode potential E^{*0} is given by [4]:

$$E_{\text{eq}} = E_{\text{Ln}(n)/\text{Ln}(0)}^0 + \frac{RT}{nF} \ln \left(\frac{a_{\text{Ln}(n)}}{a_{\text{Ln}(0)}} \right) = E_{\text{Ln}(n)/\text{Ln}(0)}^{*0} + \frac{RT}{nF} \ln X_{\text{Ln}(n)}$$

where n , R , T , and F are as defined previously; $E_{\text{Ln}(n)/\text{Ln}(0)}^0$ represents the standard potential; $X_{\text{Ln}(n)}$ and $\gamma_{\text{Ln}(n)}$ denote the concentration and activity coefficient of Ln(n) ions, respectively; and the activity of Ln metal $a_{\text{Ln}(0)}$ is unity.

Combining the Nernst equation with the definition of apparent standard potential yields:

$$E_{\text{Ln}(n)/\text{Ln}(0)}^{*0} = E_{\text{eq}} - \frac{RT}{nF} \ln X_{\text{Ln}(n)}$$

At different temperatures, a negative current was applied to the W electrode for 60 s, and the OCP relative to the reference electrode was recorded. As shown in Figure 6 [Figure 6: see original paper], each experiment produced a potential plateau representing the equilibrium potential of Nd(III)/Nd relative to the Pt reference electrode at various temperatures. Using Equation (8), the apparent standard electrode potentials of Nd(III)/Nd relative to Pt at different temperatures were calculated and listed in Table 2. The data show that the measured apparent standard potentials shift positively with increasing temperature, with decreasing absolute values. This temperature dependence follows the Nernst equation, where electrode potential correlates positively with temperature [4].

3.5 Electrolytic Separation of Nd from NdF₃ (3 wt.%)–FLiNaK Melts

The one-step, three-electron transfer reduction of Nd(III) to metallic Nd in NdF₃ (3 wt.%)–FLiNaK melts suggests the feasibility of Nd separation via electrolysis. However, as electrolysis proceeds, the concentration of electroactive

Nd(III) ions in the melt continuously decreases, and electrolysis products adsorbed on the electrode surface can hinder further Nd(III) deposition, leading to reduced current efficiency. To overcome these challenges from concentration depletion and salt adhesion, this study employed pulsed electrolysis, an effective technique for mitigating concentration polarization effects and improving current efficiency.

Figure 7a illustrates the voltage cycle used for pulsed potential electrolysis. Each 65 s pulse cycle comprises four stages: (1) application of -1.7 V for 5 s, a potential between the Li^+ reduction potential (-2.0 V vs. Pt) and the Nd(III) reduction potential (-1.65 V vs. Pt), to concentrate Nd(III) at the cathode surface; (2) application of -1.6 V for 55 s, slightly more negative than the Nd(III) reduction potential, for selective Nd deposition; (3) application of $+0.1$ V for 3 s to redissolve the loose deposit layer back into the melt; and (4) application of 0 V for 2 s to stabilize the melt system. Electrolysis was conducted for 200 cycles, and Figure 7b shows that the current remained essentially constant throughout the process, indicating that ion concentration changes from deposition did not affect the pulsed electrolysis. With relatively stable Nd(III) concentration and current density near the electrode, potential fluctuations from concentration polarization were minimal, suppressing side reactions and impurity deposition.

3.6 Electrolysis Products and Ion Concentration Changes

Cyclic voltammograms scanning the Nd redox peaks before and after electrolysis are shown in Figure 8a [Figure 8: see original paper]. Post-electrolysis, the Li^+ and impurity peaks shifted positively by approximately 62 mV, while the original Nd(III) \rightarrow Nd(0) redox peaks significantly decreased, indicating partial electrolytic separation of Nd(III) from the melt. Since peak current in cyclic voltammetry correlates with concentration, the separation efficiency can be estimated from the ratio of cathodic peak currents (i_{pc}) for Nd(III) \rightarrow Nd(0) before and after electrolysis ($i_{pc, \text{before}}/i_{pc, \text{after}}$). From Figure 8a, this ratio is -0.04698 A / -0.02239 A = 2.1, suggesting that Nd(III) concentration in the melt decreased by approximately 2.1-fold. Table 3 presents Nd(III) concentration measurements in the melt before and after electrolytic reduction, showing concentration decreases exceeding 5 mg/g depending on sampling location, demonstrating good separation efficiency.

Figure 8b shows the XRD pattern of the cathodic electrolysis product. The results indicate that Nd exists primarily in metallic form, with minor signals from NdF_3 . Peaks corresponding to LiF, KF, and NaF originate from melt contamination during sample collection and transfer. These findings preliminarily confirm the feasibility of Nd separation via pulsed electrolysis in this system.

4. Conclusions

The electrochemical behavior of NdF_3 (3 wt.%) in FLiNaK melts was systematically investigated between 873 K and 933 K using cyclic voltammetry, chronopotentiometry, and square wave voltammetry. The main conclusions are as follows:

- (1) Square wave voltammetry confirms that $\text{Nd(III)} + 3\text{e}^- \rightarrow \text{Nd(0)}$ on inert tungsten electrodes proceeds as a one-step, diffusion-controlled quasi-reversible process.
- (2) Cyclic voltammetry was used to determine diffusion coefficients of Nd(III) ions at 873 K, 893 K, 913 K, and 933 K. With increasing temperature, the redox potential of Nd(III) shifts positively and the diffusion coefficient increases.
- (3) The temperature dependence of the diffusion coefficient follows the Arrhenius equation, yielding an activation energy of $174.49 \text{ kJ} \cdot \text{mol}^{-1}$ for Nd(III) in FLiNaK melts.
- (4) Using electromotive force measurements, equilibrium potentials (E_{eq}) were obtained and used to calculate apparent standard electrode potentials (E^{*0}), which shift positively with increasing temperature.
- (5) Pulsed electrolysis of the NdF_3 -FLiNaK melt system for 3.6 hours significantly reduced Nd concentration in the melt and resulted in metallic Nd deposition on the cathode electrode.

5. References

- (1) Peng, H.; Shen, M.; Zuo, Y.; Fu, H.; Xie, L. *Journal of Nuclear Materials* **2018**, *510*, 256-264. DOI: 10.1016/j.jnucmat.2018.08.013.
Peng, H.; Ji, N.; Huang, W.; Gong, Y.; Santos, R. M. *International Journal of Energy Research* **2023**, *2023*, 1-14. doi: 10.1155/2023/4447405.
Galashev, A. *Applied Sciences* **2023**, *13*(2), 1085. doi: 10.3390/app13021085.
- (2) Bruno, J. E., R. C. *Elements* **2006**, *2*(6), 343-349. doi:10.2113/gselements.2.6.343.
A. A. Lizin, S. V. T., O. E. Gnevashov, R. K. Gazizov, A. G. Osipenko, M. V. Kormilitsyn, A. A. Baranov, L.V. Zaharova, V.S. Naumov, L.I. Ponomarev. *At. Energy*. **2013**, *115*, 11-17. doi:10.1007/s10512-013-9740-9.
- (3) Zhao, Z.; Geng, J.; Cheng, Z.; Li, W.; Dou, Q.; Zhang, L.; Li, Q. *RSC Adv* **2024**, *14*(23), 15994-16000. doi: 10.1039/d4ra02114b.
- (4) Fusselman, S. P., Roy, J. J., Grimmer, D. L., Grantham, L. F., Krueger, C. L., Nabelek, C. R., Takahashi, N. *Journal of the Electrochemical Society* **1999**, *146*(7), 2573. doi:10.1149/1.1391974.

- (5) Abbasalizadeh, A.; Seetharaman, S.; Venkatesan, P.; Sietsma, J.; Yang, Y. *Electrochimica Acta* **2019**, *310*, 146–152. doi: 10.1016/j.electacta.2019.03.161.
Periyapperuma, K.; Sanchez-Cupido, L.; Pringle, J. M.; Pozo-Gonzalo, C. *Sustainable Chemistry* **2021**, *2*(3), 550–563. doi: 10.3390/suschem2030030.
- (6) Gong, W.; Wang, X.; Huang, C.; Wang, X.; Fu, Y. *Annals of Nuclear Energy* **2024**, *199*, 110362. doi: 10.1016/j.anucene.2024.110362.
- (7) Zhou, G.Y.; Wu, M.; Bao, C.; Zhang, N.; Tu, S. T. *Nuclear Engineering and Design* **2024**, *421*, 113097. doi: 10.1016/j.nucengdes.2024.113097.
- (8) Yamana, H.; Park, B. G.; Shirai, O.; Fujii, T.; Uehara, A.; Moriyama, H. *Journal of Alloys and Compounds* **2006**, *408–412*, 66–70. DOI: 10.1016/j.jallcom.2005.04.104.
- (9) Tang, H.; Pesic, B. *Journal of Nuclear Materials* **2015**, *458*, 37–44. doi: 10.1016/j.jnucmat.2014.11.084.
- (10) Vandarkuzhali, S.; Chandra, M.; Ghosh, S.; Samanta, N.; Nedumaran, S.; Prabhakara Reddy, B.; Nagarajan, K. *Electrochimica Acta* **2014**, *145*, 86–98. doi: 10.1016/j.electacta.2014.08.069.
- (11) Castrillejo, Y.; Bermejo, M. R.; Barrado, E.; Martínez, A. M.; Díaz, A. *Electroanalytical Journal* **2003**, *10.1016/s0022-0728(03)00092-5*.
- (12) Liu, K. L.; Y. L.; Chai, Z. F.; Shi, W. Q. *Separation and Purification Technology* **2021**, *265*, 118524. doi: 10.1016/j.seppur.2021.118524.
- (13) Novoselova, A.; Smolenski, V. *Electrochimica Acta* **2013**, *87*, 657–662. doi: 10.1016/j.electacta.2012.09.064.
- (14) Stefanidaki, E. H., C.; Kontoyannis, C. *Electrochimica Acta* **2001**, *46*(17), 2665–2670. doi:10.1016/S0013-4686(01)00489-3.
- (15) Moriyama, H., Seshimo, T., Moritani, K., Ito, Y., & Mitsugashira, T. *Journal of Alloys and Compounds* **1994**, *213*, 354–359. doi:10.1016/0925-8388(94)90930-X.
- (16) Rault, L.; Heusch, M.; Allibert, M.; Lemort, F.; Deschanel, X.; Boen, R. *Nuclear Technology* **2017**, *139*(2), 167–174. doi: 10.13182/nt02-a3311.
- (17) Gibilaro, M.; Massot, L.; Chamelot, P.; Taxil, P. *Journal of Nuclear Materials* **2008**, *382*(1), 39–45. doi: 10.1016/j.jnucmat.2008.09.004.
- (18) Chamelot, P.; Massot, L.; Hamel, C.; Nourry, C.; Taxil, P. *Journal of Nuclear Materials* **2007**, *360*(1), 64–74. doi: 10.1016/j.jnucmat.2006.08.015.
- (19) SouČEK, P.; LisÝ, F.; TulÁČKovÁ, R.; UhlÍŘ, J.; MrÁZ, R. *Journal of Nuclear Science* **2005**, *10.1080/18811248.2005.9711054*.
- (20) Yang, Q.; Ge, J.; Wang, Y.; Zhang, J. *Nuclear Technology* **2020**, *206*(11), 1769–1777. doi: 10.1080/00295450.2020.1757976.

- (21) Dauphin-Ducharme, P.; Arroyo-Curras, N.; Kurnik, M.; Ortega, G.; Li, H.; Plaxco, K. W. *Langmuir* **2017**, *10.1021/acs.langmuir.7b00359*.
- (22) Y. Liu.; Y. Liu.; L. Wang.; S. Jiang.; D. Wang.; Z. Liu.; W. Shi. *ACS Sustainable Chemistry & Engineering* **2023**, *11*, 8161–8172.
- (23) Mehta, A., Barker, G. C. *Reports on Progress in Physics* **1994**, *57*(4), 383. doi:10.1088/0034-4885/57/4/002.
- (24) Smith, N. D.; Lombardo, S.; Shang, S.L.; Liu, Z.K.; Kim, H. *Journal of The Electrochemical Society* **2023**, *170*(6), 066505. doi: 10.1149/1945-7111/acd6c1.
- (25) Laidler, K. *Journal of Chemical Education* **1984**, *61*(6), doi:10.1021/ed061p494.
- (26) Liu, Z.; Lu, G.; Yu, J. *Separation and Purification Technology* **2021**, *268*, 118354. doi:10.1016/j.seppur.2021.118354.
- (27) Dowben, S. A.; Steppan, J.; Choi, S.; Bae, S. E.; Dale, O.; Meaders, T.; Gonzalez, M.; Perez, P.; Simpson, M. F. *Journal of The Electrochemical Society* **2024**, *171*(2), 027501. doi: 10.1149/1945-7111/ad2151.
- (28) Lichtenstein, T.; Patricelli, C. V.; Hawthorne, K. L. *Journal of The Electrochemical Society* **2023**, *170*(6), 066506. doi: 10.1149/1945-7111/acd9f2.

Note: Figure translations are in progress. See original paper for figures.

Source: ChinaXiv –Machine translation. Verify with original.